Journal of the Indian Chemical Society 102 (2025) 101620

Contents lists available at ScienceDirect

Journal of the Indian Chemical Society

journal homepage: www.journals.elsevier.com/journal-of-the-indian-chemical-society

Influence of temperature and selenium substitution on electrical and dielectric characteristics of $CoFe_2O_4$ nanoparticles

B. Ünal [a], A. Baykal [b,c,*], M.A. Almessiere [d,e,**], A. Mihmanlı [f]

[a] Department of Electrical and Electronics Engineering, Faculty of Engineering and Architecture, İstanbul Gelisim University, Avcılar, İstanbul, Türkiye
[b] Food Engineering Department, Faculty of Engineering, Istanbul Aydin University, 34295, Florya, Istanbul, Türkiye
[c] Basic Pharmacy Department, Pharmacy Faculty, Istanbul Aydin University, 34295, Florya, Istanbul, Türkiye
[d] Department of Biophysics, Institute for Research and Medical Consultations (IRMC), Imam Abdulrahman Bin Faisal University, 31441, Dammam, Saudi Arabia
[e] Department of Physics, College of Science, Imam Abdulrahman Bin Faisal University, 31441, Dammam, Saudi Arabia
[f] Faculty of Dentistry, Gelişim University, No:1, 34310, Avcılar, Istanbul, Türkiye

ARTICLE INFO

Keywords:
$CoFe_2O_4$
Electrical/dielectric properties
Hydrothermal synthesis
Se substitution
AC/DC conductivity

ABSTRACT

This study investigates the influence of Se^{4+} ion substitution on the electrical and dielectric properties of $CoFe_2O_4$ nanoparticles ($CoFe_{2-4x}Se_{3x}O_4$ ($x \leq 0.1$) (NPs)) synthesized via a hydrothermal method. The electrical and dielectric characteristics were analyzed using a Novocontrol dielectric impedance analyzer. Results indicate that activation energies (E_a) remain stable at approximately 600 meV at higher temperatures ($T \geq 45$ °C) but decrease significantly at lower temperatures, ranging from 300 meV ($x = 0.02$) to 20 meV ($x = 0.08$). A sharp reduction in DC conductivity, from 1.2 *nS/cm* ($x = 0.04$) to 0.27 *nS/cm* ($x = 0.08$), suggests enhanced electron mobility at this substitution level. AC conductivity exhibits strong frequency dependence, increasing from 0.15 *nS/cm* at 1 kHz to 0.13 *μS/cm* at 1 MHz for $x = 0.08$ at room temperature. Dielectric constant (ε') and loss (ε'') values exhibit significant variation with frequency, with ε' reaching a maximum of 3.95 at 100 Hz for $x = 0.08$, reflecting enhanced polarization effects. Se^{4+} substitution also increases the real part of the electrical modulus (ReM) to 0.99 and the imaginary part (ImM) to 0.40 for $x = 0.10$, indicating improved energy storage and dissipation capabilities. The ImZ/ReZ ratio analysis reveals shifts in conduction mechanisms and polarization effects, with a notable transition at $x = 0.04$. Cole-Cole plots suggest multiple relaxation processes influenced by temperature and substitution levels, with relaxation times decreasing from 13 ms (70 °C) to 0.76 ms (120 °C) for $x = 0.02$. This study highlights the potential of Se^{4+}-substituted Co-SFs for applications in electronic devices, particularly in energy storage and dissipation systems, and underscores the need for combined experimental and theoretical approaches to optimize these materials for advanced technological applications.

1. Introduction

Spinel ferrites (SFs) are important classes of magnetic materials due to their intrinsic magnetic, electrical and optical properties like high permeability, high saturation magnetization, low coercivity, high electrical resistivity, low magnetostriction, high curie T, low anisotropy, easy and cheap synthesis etc. [1,2]. They have wide range of applications, millimeter wave integrated circuitry, antenna rods, drug delivery systems, transducers, permanent magnets, magnetic recorders, traNPormer cores, memory chips, activators, computer components, and microwave devices [3–5].

$CoFe_2O_4$ nanoparticles (NPs) have a fascinating inverse cubic spinel structure [6]. While the Co^{2+} cations occupy Oh site, Fe^{3+} cations are equally dispersed in inverse spinel between Td and Oh sites. $CoFe_2O_4$ is one of the most mostly studied spinel ferrite due to its moderate saturation magnetization, high Curie T, high magneto crystalline anisotropy, high Néel T and etc. [7,8]. Additionally, $CoFe_2O_4$ was proved to be good dielectric material due to its high dielectric permittivity (ε) hence it is currently being used in energy storage devices, tomography, MRI (magnetic resonance imaging) as contrast agents, and in cancer treatment, actuators, sonars, microwave absorber, micromotors and etc. [9,10]. The low conductivity and high electrical resistivity make this

* Corresponding author. Food Engineering Department, Faculty of Engineering, Istanbul Aydin University, 34295, Florya, Istanbul, Türkiye.
** Corresponding author. Department of Biophysics, Institute for Research and Medical Consultations (IRMC), Imam Abdulrahman Bin Faisal University, 31441, Dammam, Saudi Arabia.
E-mail addresses: abdulhadibaykal@aydin.edu.tr (A. Baykal), malmessiere@iau.edu.sa (M.A. Almessiere).

https://doi.org/10.1016/j.jics.2025.101620
Received 18 November 2024; Received in revised form 28 January 2025; Accepted 9 February 2025
Available online 11 February 2025

nanomaterial as attractive candidate in the electrical field. Moreover, $CoFe_2O_4$ NPs is known as highly attractive magnetic materials among other oxides due to their specific properties and low-cost production. By using $CoFe_2O_4$ NPs as an alternative to Fe_3O_4 NPs, small-sized biocompatible devices can be assembled, which can lead to the advancement of cellular intake as well as prevention of the reticuloendothelial system. On the other hand, appropriate staying time and low dose in the patient body are interesting for in vivo applications of $CoFe_2O_4$ NPs [11,12]. $CoFe_2O_4$ NPs have also perfect surface area, which allows for better interaction with microbial cells, leading to enhanced antimicrobial activity [13].

Changing the cation distribution by substituting Fe^{3+} or Co^{2+} with different elements (transition metal ions or rare earth metal ions) will affect cobalt ferrite's both magnetic and electrical properties [14]. The replacement of Fe^{3+} ions by RE^{3+} ions during substitution process can improve the magneto-optical and electrical properties of host $CoFe_2O_4$ NPs. During this substitution process, the substituted RE^{3+} ion interacts with Fe^{3+} ions by producing some cation deficiencies in single-phase cubic structures, further tunning the conduction mechanism in spinel ferrite NPs [15]. S. Ravi Kumar et al. reported that the doping of Nd^{3+} at Fe^{3+} bimetallic ions into $Co_{0.5}Ni_{0.5}Fe_2O_4$ structure improved its DC resistivity [16]. Xi et al. [17] studied on the effect RE substitution on magnetostriction characteristics of $CoFe_2O_4$ prepared from spent Li-ion batteries and concluded that Fe^{3+} replacement by RE^{3+} in spinel structure can produce desirable modifications in microstructure and characteristics.

Unfortunately, the number of studies based on Se substitution is so limited. A. Baykal et al. [18] studied the effect of Se^{4+} ion substitution on the magnetic features of $Ni_{0.6}Cu_{0.2}Zn_{0.2}Fe_2O_4$ nanospinel ferrites and reported that high Se doping level resulted in a drop in the magnetic properties (Ms, Mr, and *nB*). Almessiere et al. [19] compared the magnetic properties of Se^{4+} doped $CoFe_2O_4$ fabricated via hydrothermal and sol-gel routes and concluded that the choice of synthesis approach can affect the magnetic parameters of host $CoFe_2O_4$ NPs. Bide et al. [20] reported high catalytic activity of Se doped graphene/$CoFe_2O_4$ for dehydrogenation of formic acid.

In this study, the effect of Se doping on the electrical and dielectric behavior of hydrothermally synthesized $CoFe_2O_4$ ($x \leq 0.1$) NPs have been investigated.

2. Experimental

2.1. Synthesis and characterization

The details of the synthesis of $CoFe_{2-4x}Se_{3x}O_4$ NPs via hydrothermal method has been already given in our previous publication [19].

All the samples were prepared in pellets and the dielectric measurements were performed using double parallel electrodes such as sandwich form. For electrical measurement, silver paste was applied as electrodes on both sides of the pellets. The electrical properties were studied by impedance spectroscopy (IS) measurements performed on the sintered materials (All the samples were prepared in pellets) using Novocontrol concept 50 system in the $1–10^6$ Hz frequency range. The IS measurements were performed at different temperatures where the temperature was controlled by the Quatro cryosystem.

3. Results & discussion

3.1. Structure and morphology

The XRD powder patterns of $CoFe_{2-4x}Se_{3x}O_4$ NPs confirmed the formation of SFs with absence of any secondary phase and have been indexed with cubic spinel structure according (ICDD card no:96-591-0064), as reported in detail in previous paper [19].

3.2. Electrical properties

The electrical properties of $CoFe_{2-4x}Se_{3x}O_4$ NPs have been thoroughly examined to determine how Se^{4+} ion substitution impacts conductivity and related characteristics. The substitution significantly increases electrical conductivity, which is attributed to changes in the electronic band structure, defect concentrations, and charge carrier mobility within the crystal lattice [21].

As Se^{4+} ions replace Cobalt ions, additional charge carriers are introduced, leading to enhanced conductivity, reduced scattering of charge carriers, and improved mobility. Furthermore, the T dependence of conductivity is notably affected by Se^{4+} ion substitution, especially near the transition T (T_{trans}), where magnetic ordering and spin configurations influence electrical behavior [22,23]. Se^{4+} ion substitution can also cause a shift in T_{trans}, thereby impacting electrical properties across various Ts.

Understanding these electrical properties is essential for their potential applications in electronics, sensors, and energy conversion devices. $CoFe_{2-4x}Se_{3x}O_4$ NPs are particularly promising for use in magnetic sensors, electromagnetic shielding, and high-*f* circuits, where their tailored electrical conductivity and magnetic properties are advantageous [19]. Consequently, Se^{4+} ion substitution in Co-SFs leads to significant modifications in conductivity, resistivity, and T-dependent behavior, making these materials highly suitable for various technological applications that require specific electrical characteristics for optimal functionality and efficiency [24,25].

3.2.1. AC conductivity

The AC conductivity of $CoFe_{2-4x}Se_{3x}O_4$ NPs has been extensively studied to understand how Se^{4+} ion substitution influences the electrical behavior of the ferrite material across varying frequencies. This *f*-dependent AC conductivity offers valuable insights into the interaction between charge carriers and the intra-grains [24].

Fig. 1 presents a 3D plot of the *f* and T-dependent conductivity of $CoFe_{2-4x}Se_{3x}O_4$ NPs hydrothermal, covering Se^{4+} ion substitution ratios in the range of $x = 0.02$ to 0.10. The AC conductivity generally increases with rising *f*, with the rate of increase varying based on the substitution ratios. At low frequencies, T-dependent conductivity is more pronounced compared to the high-*f* range. Notably, for $x = 0.04$, the conductivity exhibits a distinctive trend in the mid-*f* region, likely due to the structural interactions between Se ion and Fe or Co ions.

Typically, at low frequencies, AC conductivity increases with higher Se^{4+} ion content due to enhanced charge carrier mobility and reduced scattering at defects and grain boundaries. However, at higher frequencies, the AC conductivity may decrease or plateau, influenced by polarization effects, relaxation processes, and dielectric losses.

Se^{4+} ion substitution also significantly affects the T dependence of AC conductivity, especially near the T_{trans}, where magnetic transitions lead to notable changes in conductivity [22,23]. These shifts are tied to changes in magnetic domain dynamics and spin interactions [19], which are crucial for understanding the Ea and thermal behavior of charge carriers.

The analysis of AC conductivity in these materials often employs Jonscher's universal power law, where the *f* exponent provides insights into the conduction mechanism [26]. The Se^{4+} ion substitution can alter the electronic environment by introducing localized states and changing the cation distribution, which in turn affects the AC conductivity.

Studies indicate that Se^{4+} ion substitution generally leads to a decrease in overall AC conductivity, particularly at lower frequencies. This reduction is possibly due to increased resistive grain boundaries or a decrease in Fe^{2+} ions, which are essential for the hopping conduction mechanism. At higher frequencies, the behavior can vary depending on how Se^{4+} ion influences polarization or hopping mechanisms.

Understanding AC conductivity is crucial for applications in telecommunications, electromagnetic devices, and high-*f* circuits [19,22,24]. The *f*-dependent behavior of AC conductivity allows for the

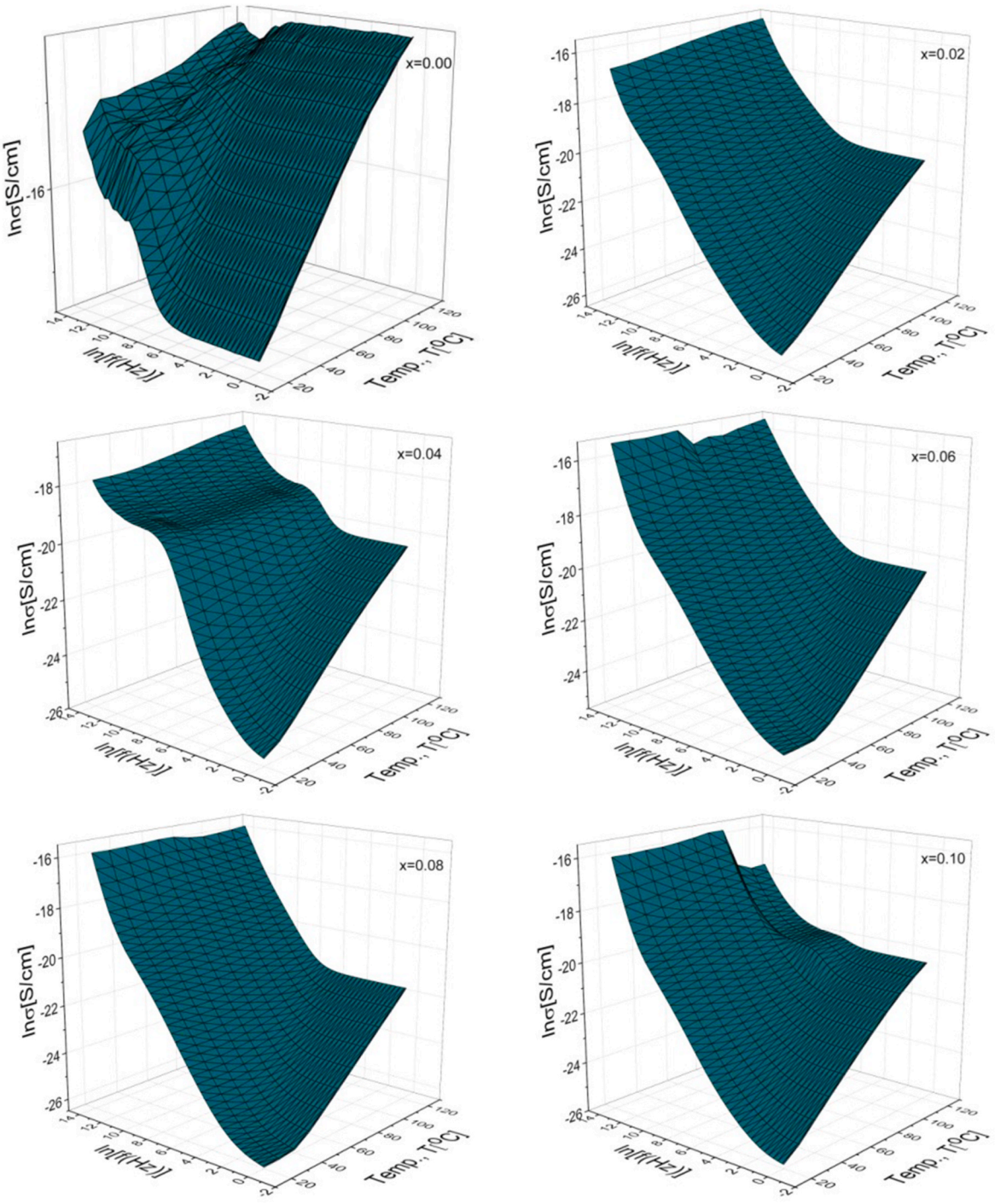

Fig. 1. 3D plot of the *f* and T dependent conductivity of $CoFe_{2-4x}Se_{3x}O_4$ NPs.

tailoring of the response of the NPs to specific *f* ranges, optimizing performance in applications such as antennas, filters, and electromagnetic shielding materials [23–25]. Consequently, Se^{4+} ion substitution in Co-SFs leads to complex changes in AC conductivity, reflecting modifications in charge carrier mobility, dielectric properties, and *f*-dependent behavior. These changes are essential for designing materials with controlled electrical characteristics for various technological applications.

3.2.2. DC conductivity and activation energy (E_a)

The DC conductivity and Ea of $CoFe_{2-4x}Se_{3x}O_4$ NPs have been extensively studied to understand how Se^{4+} ion substitution influences charge carrier transport and the energy required for conduction. In Co-SFs, DC conductivity typically occurs through the hopping of electrons between Fe^{3+} and Fe^{2+} ions. Se^{4+} ion substitution can significantly impact this mechanism by introducing additional charge carriers and modifying the Fe^{2+}/Fe^{3+} ratio. As selenium content increases, DC conductivity generally increases due to the enhanced mobility of charge carriers and reduced E_a barriers.

Fig. 2 presents both 2D and 3D Arrhenius plots showing the DC conductivity of $CoFe_{2-4x}Se_{3x}O_4$ NPs (hydrothermally synthesized) across various Se^{4+} ion substitution ratios. At Ts above 45 °C, the activation energies for all substitution ratios in these Co-SFs remain almost constant, varying between approximately 600 and 700 meV. At lower Ts,

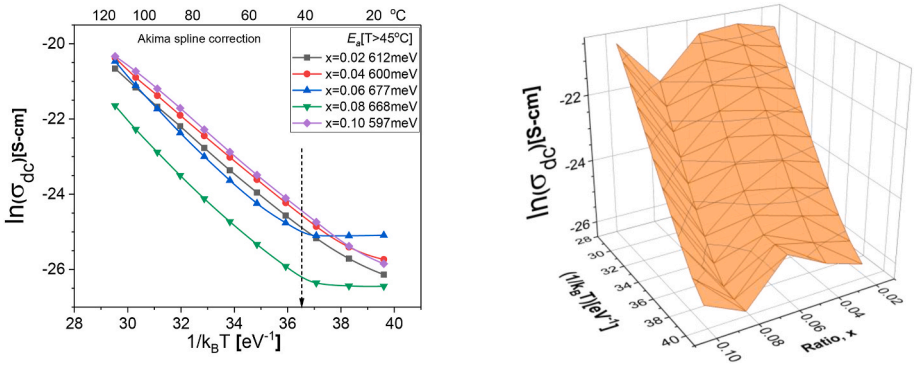

Fig. 2. Arrhenius plot showing the DC conductivity of $CoFe_{2-4x}Se_{3x}O_4$ NPs, illustrated in both 2D and 3D plots.

these values decrease significantly, depending on the substitution ratios.

The E_a, representing the energy barrier that charge carriers must overcome to move through the material, tends to fluctuate with Se^{4+} ion substitution. This fluctuation indicates easier movement of charge carriers, thereby enhancing conductivity. The fluctuation in Ea is often attributed to changes in the electronic structure near the Fermi level and alterations in the density of states associated with Se ions.

T-dependent studies of DC conductivity reveal that as T increases, thermal energy helps charge carriers overcome activation barriers, leading to increased conductivity. However, Se^{4+} ion substitution can also introduce complexities, such as cation redistribution and increased grain boundary resistivity, which may lead to a decrease in DC conductivity under certain conditions. This reduction is often observed when selenium disrupts typical electron hopping paths or when secondary phases are introduced, affecting the overall electrical properties of the material.

Understanding these effects is crucial for designing and optimizing materials for applications such as sensors, electromagnetic devices, and electronic components, where specific electrical properties are required. In summary, Se^{4+} ion substitution in Co-SFs alters DC conductivity and Ea by modifying charge carrier concentrations, electronic band structures, and activation barriers. These changes are critical for optimizing the performance of ferrite material in various technological applications requiring tailored electrical and magnetic characteristics [21–23].

3.3. Dielectric properties

The dielectric properties of $CoFe_{2-4x}Se_{3x}O_4$ NPs have been extensively studied to understand the effects of Se^{4+} ion substitution on the dielectric behavior of ferrites. The AC conductivity of the material is closely linked to its dielectric properties, particularly the dielectric constant (ε') and the loss tangent (tanδ), both of which are influenced by Se^{4+} ion substitution. These changes affect the NPs' response to alternating electric fields, impacting their capacitive and resistive components of impedance.

3.3.1. Dielectric constant

In $CoFe_{2-4x}Se_{3x}O_4$ NPs, the dielectric constant generally increases slightly with higher Se ion content up to a certain threshold, beyond which it may decrease due to structural changes or saturation effects. This behavior is heavily influenced by the distribution of cations and anions within the intra-grains, as Se^{4+} ion substitution alters this distribution, affecting polarization mechanisms such as dipolar, electronic, ionic, and interfacial (space charge) polarization.

Fig. 3 illustrates the 3D representation of the dielectric constant of $CoFe_{2-4x}Se_{3x}O_4$ NPs, synthesized hydrothermally, as a function of *f* and T. The dielectric constant is observed to be T-dependent across all substitution ratios for frequencies up to 3.0 MHz. While this T dependence varies slightly with *f* for most substitution ratios, it shows a notable change for x = 0.10 at Ts above approximately 80 °C. Notably, at lower Ts, the dielectric constant exhibits greater T independence.

Se^{4+} ion substitution also impacts the dependence of the dielectric constant. At low frequencies, the dielectric constant tends to be higher due to dominant space charge and dipolar polarization. However, Se^{4+} ion substitution may reduce the dielectric constant by disrupting dipole alignment or increasing the resistivity of grain boundaries, which hinders the mobility of charge carriers. As *the increase*, the dielectric constant typically decreases, and Se^{4+} ion substitution may accelerate this reduction by introducing defects that impair polarization mechanisms.

T dependence is another critical factor, with the dielectric constant increasing with T due to enhanced alignment of dipoles with the electric field. However, Se^{4+} ion substitution can modify this trend by altering the Ea required for polarization, potentially lowering the dielectric constant by introducing defects that inhibit dipole orientation or reduce the concentration of mobile charge carriers.

Literature findings generally report a decrease in the dielectric constant with Se^{4+} ion substitution, attributed to a reduction in space charge polarization and increased resistivity at grain boundaries. This decrease is often accompanied by more pronounced *f* dispersion and a corresponding decrease in AC conductivity, reflecting the interconnected nature of these properties [27,28].

In comparison with pure Co-SF, Se^{4+} ion -substituted variants consistently show a reduced dielectric constant across all frequencies and Ts. The reduction is more significant at lower frequencies, where space charge and dipolar polarization are most active. This suggests that Se^{4+}ion-substituted ferrites may be less suitable for applications requiring high dielectric storage but could be beneficial in applications where a lower dielectric constant and higher stability are desired, such as in specific types of sensors or electronic devices [23,24,29]. Accordingly, $CoFe_{2-4x}Se_{3x}O_4$ NPs generally leads to a decrease in the dielectric constant, influenced by changes in polarization mechanisms, increased grain boundary resistivity, and the introduction of defect states. These modifications have important implications for the material's performance in various technological applications.

3.3.2. Dielectric loss

Dielectric loss in $CoFe_{2-4x}Se_{3x}O_4$ NPs is influenced by the intrinsic properties of spinel ferrites and the specific effects of Se^{4+} ion substitution. Spinel ferrites, such as $CoFe_2O_4$, are characterized by high resistivity and *f*-dependent dielectric behavior, making dielectric loss a key factor in evaluating their potential for electronic applications.

When Se^{4+} ions substitute for oxygen or other ions in the spinel intragrain lattice, they modify the electronic distribution and local structure, impacting both the dielectric constant and dielectric loss. Selenium, which can exist in different valence states (e.g., Se^{4+} or Se^{6+}), introduces charge compensation mechanisms that affect the dielectric behavior of ferrite material. This substitution may also introduce defects or lattice distortions, influencing polarization mechanisms such as dipole, ionic, and space charge polarization.

Hydrothermal synthesis of $CoFe_{2-4x}Se_{3x}O_4$ NPs is particularly

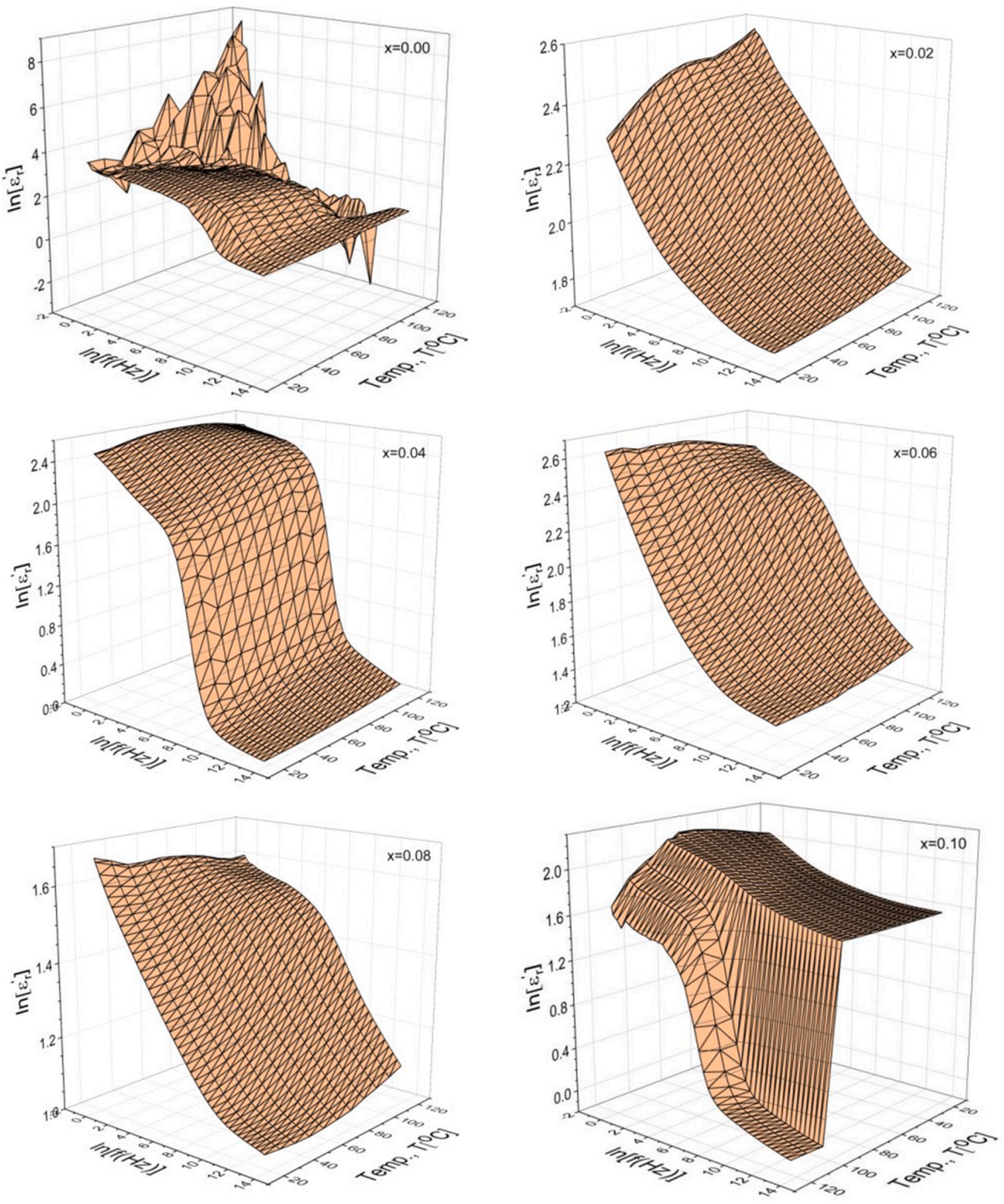

Fig. 3. 3D plot of the *f* and T dependent dielectric constant of $CoFe_{2-4x}Se_{3x}O_4$ NPs.

important because it yields well-crystallized materials with controlled grain size and morphology, leading to high purity and uniform phase formation. These factors are essential for consistent dielectric behavior. Generally, in spinel ferrites, dielectric tangent loss decreases with increasing *f* due to the lag in polarization processes. However, in Se^{4+}ion-substituted systems, this trend may shift because of reformed conduction mechanisms or defect structures introduced by Se^{4+} ions.

Fig. 4 presents a 3D representation of the dielectric loss of $CoFe_{2-4x}Se_{3x}O_4$ NPs, synthesized hydrothermally, as a function of *f* and T. The dielectric loss increases with T at low *f*s, but this T dependence decreases with increasing *f*. The degree of T dependence varies with the substitution ratios, notably forming a valley along the *f* axis in the mid-*f* region for x = 0.04 and a peak along the T axis in the high-*f* region for x = 0.10.

Dielectric loss is also T-dependent, with peaks often reported at specific Ts. Se^{4+} ion substitution can shift these peaks or change their intensity, either reducing dielectric loss by stabilizing the spinel structure or increasing it by introducing additional relaxation mechanisms or defect states. Comparative studies between Se^{4+} ion-substituted and non-substituted ferrites demonstrate the significant Se^{4+} ion influence on dielectric loss. By controlling the synthesis conditions and the degree of Se^{4+} ion substitution, it is possible to fine-tune dielectric loss to optimize the spinel ferrite material for specific high-*f* applications, such as inductors, traNPormers, and microwave devices [18,19]. Hence, Se^{4+} ion substitution in Co-SFs significantly impacts dielectric loss by modifying the lattice structure, varying polarization mechanisms, and potentially introducing new defect states. The hydrothermal synthesis

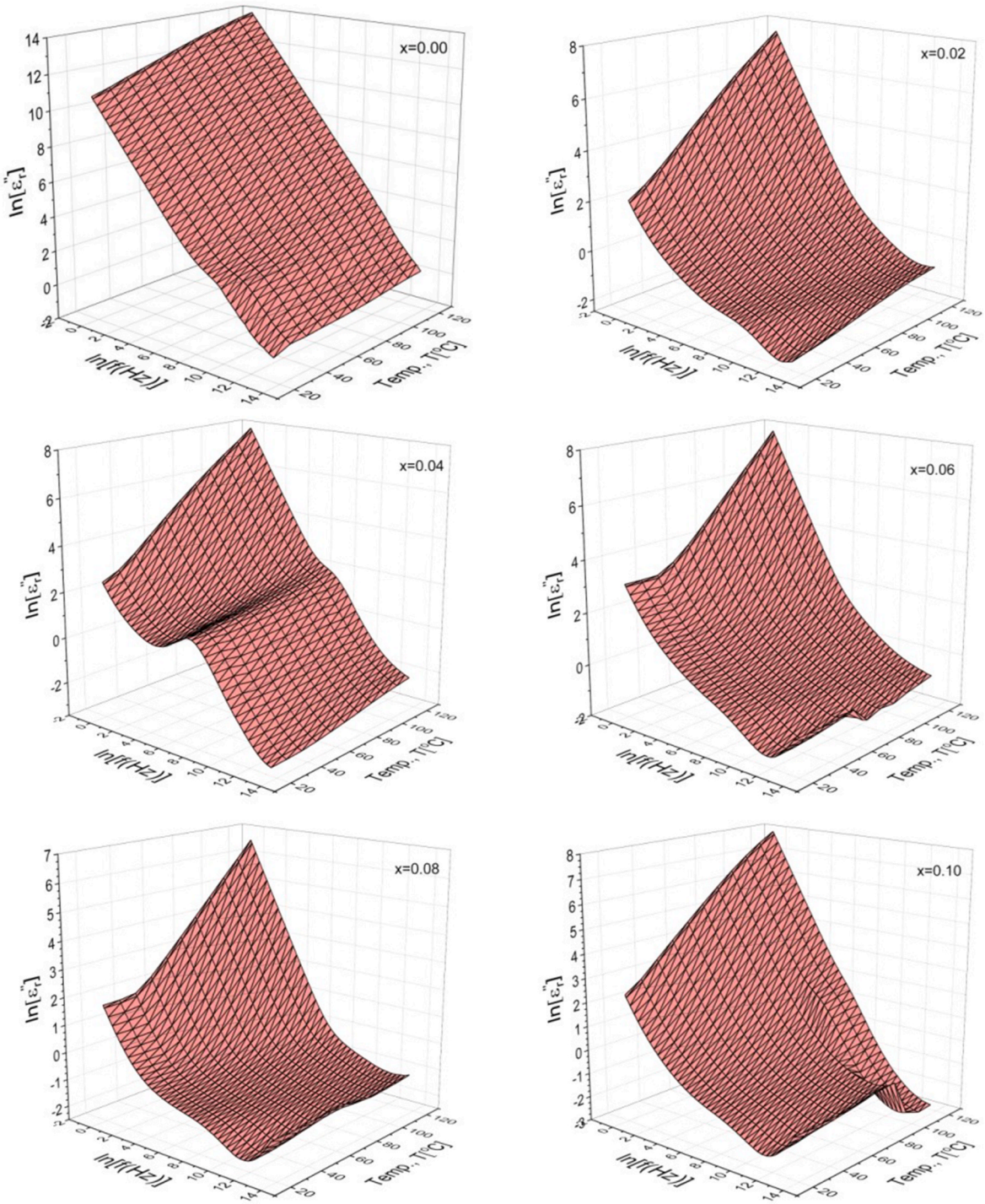

Fig. 4. 3D plot of the *f* and T-dependent dielectric loss of $CoFe_{2-4x}Se_{3x}O_4$ NPs.

process plays a crucial role in determining these properties, and the resulting *f* and T dependence of dielectric loss is vital for optimizing the material application in electronic devices.

3.3.3. Dissipation factor

The dissipation factor, also known as the loss tangent (tanδ), is a crucial parameter that measures the energy loss as heat when a material is exposed to an alternating electric field. In $CoFe_{2-4x}Se_{3x}O_4$ NPs, several factors, including lattice microstructural structure changes and polarization mechanisms by Se^{4+} ion substitution and hydrothermal synthesis, affect the dissipation factor.

Fig. 5 presents a 3D plot of the dissipation factor of $CoFe_{2-4x}Se_{3x}O_4$ NPs, synthesized hydrothermally, with respect to *f* and T for Se ion substitution ratios ranging from x = 0.02 to 0.10. The dissipation factor shows a notable change along the *f* axis for x = 0.04, while the other Co-NPs exhibit the expected regular trends. Typically, the dissipation factor increases with T at low *f*s, while it remains almost constant at high *f*s. It is also observed that T dependence decreases with increasing *f*. The *f* dependence of the dissipation factor changes with T for x = 0.10, while a slight change in the dissipation factor along the T axis is observed for x = 0.06.

Se^{4+} ion substitution in Co-NPs typically leads to a lower dielectric

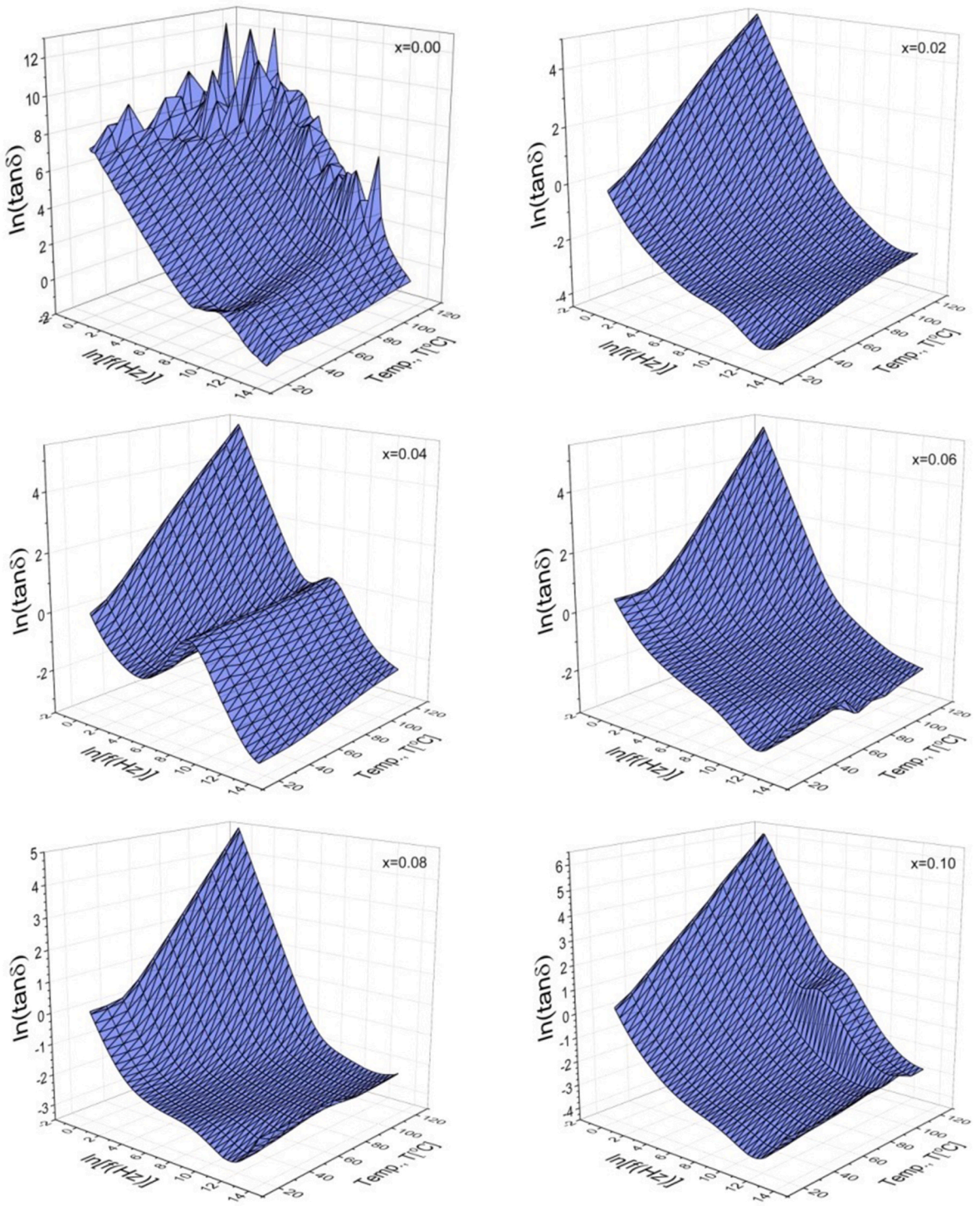

Fig. 5. 3D plot of the *f* - and T-dependent dissipation factor of $CoFe_{2-4x}Se_{3x}O_4$ NPs.

constant, which can correlate with higher dielectric loss, especially at low frequencies due to increased grain boundary effects. This substitution alters the spinel intra-grain lattice by replacing oxygen or metal cations, which changes the local electric field environment and introduces defects that affect the polarization mechanisms within the ferrite material. Consequently, Se ion substitution impacts the dissipation factor by influencing charge carrier mobility and relaxation processes.

Generally, tanδ could be modified with Se^{4+} ion substitution, a trend attributed to reduced defect concentrations and improved crystallinity of intra-grains, which are often achieved through hydrothermal synthesis. This synthesis method produces materials with controlled grain size and uniform microstructure, resulting in fewer defects and impurities, and therefore, lower dissipation factors. High purity and crystallinity reduce defect-related losses, minimizing energy dissipation.

The dissipation factor is *f* -dependent, typically decreasing with increasing *f* due to the reduced response of dipoles to the alternating field. At lower frequencies it tends to be higher because of significant polarization and conduction losses. Se^{4+} ion substitution may shift the *f* at which the dissipation factor peaks, often lowering it at higher

frequencies by reducing dielectric and conduction losses.

T also plays a significant role, as the dissipation factor varies with T, with attainable peaks at certain Ts due to increased polarization activity or carrier mobility. Se^{4+} ion substitution can shift or suppress these peaks, stabilizing the dielectric behavior across a range of Ts.

Studies comparing Se^{4+} ion-substituted ferrites with non-substituted ones often highlight that Se^{4+} ion substitution modifies the dissipation factor by enhancing dielectric stability and decreasing defect-related losses. This enhancement in the dissipation factor is particularly advantageous for high-*f* applications such as antennas, inductors, and traNPormers, where minimal energy loss is crucial [23,25]. Consequently, the dissipation factor of Se^{4+} ion-substituted Co-NPs, prepared via hydrothermal synthesis, is influenced by modifications in lattice structure, polarization mechanisms, and microstructure. Se^{4+} ion substitution generally enhances the dissipation factor by reducing conduction and polarization losses, especially at higher frequencies, making these materials more suitable for high-*f* and high-efficiency electronic and magnetic applications [28,29].

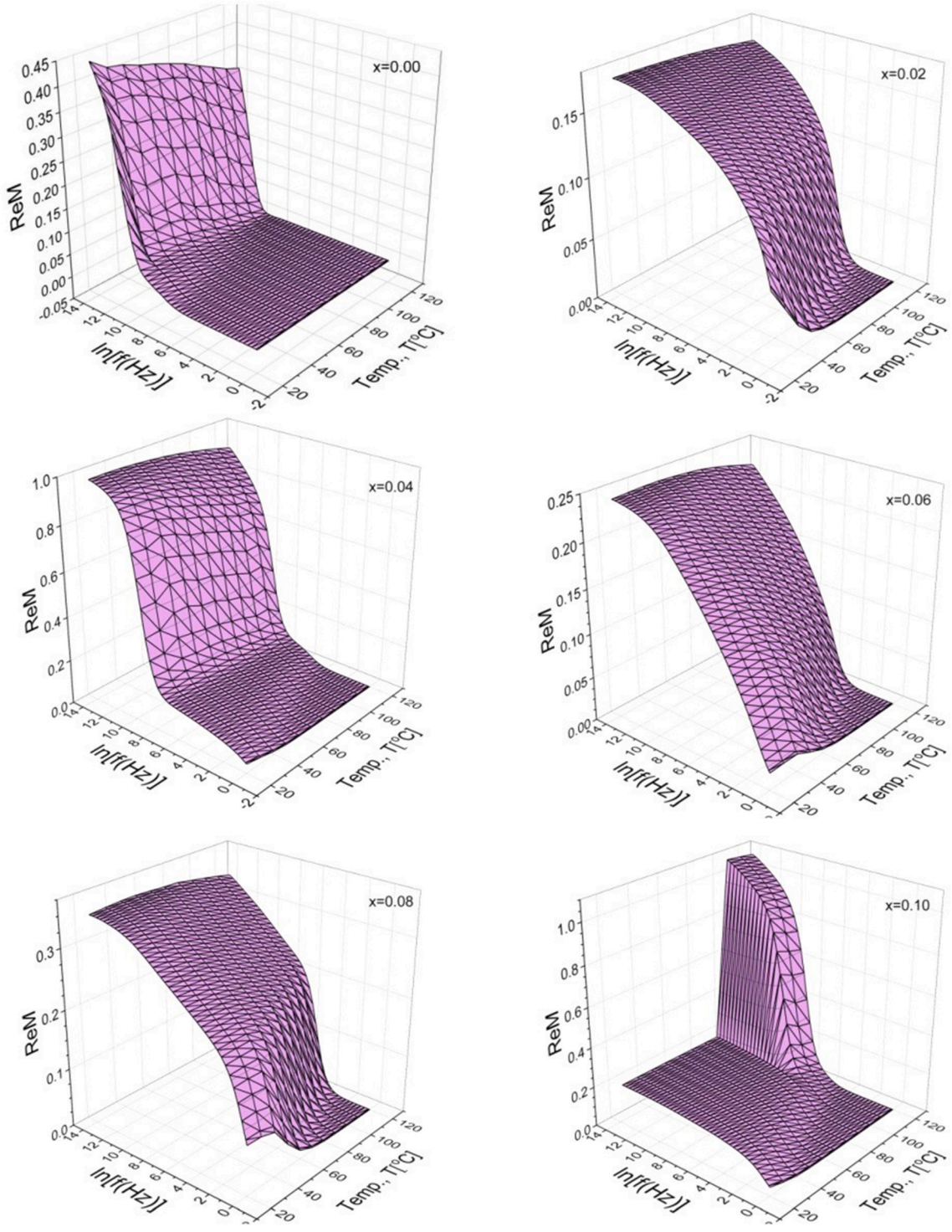

Fig. 6. 3D plot of the *f* - and T-dependent real modulus (ReM) of $CoFe_{2-4x}Se_{3x}O_4$ NPs.

3.4. Electrical complex modulus

Analyzing the electric modulus behavior of $CoFe_{2-4x}Se_{3x}O_4$ NPs, typically synthesized via hydrothermal methods, involves understanding how the dielectric properties of ferrites are affected by selenium substitution. The electric modulus (M*) is a complex quantity that gives insight into the relaxation dynamics and electrical conductivity mechanisms in materials.

Co-SFs has a cubic spinel structure, where Co^{2+} ions typically occupy the tetrahedral (A) or octahedral (B) sites, and Fe^{3+} ions are distributed between these sites. Substituting Se^{4+} ion into the spinel structure might replace Fe^{3+} ions, leading to changes in the cation distribution between A and B sites, which can significantly influence the electrical properties of the material. The electric modulus is defined as $M^*(\omega) = \frac{1}{\varepsilon^*(\omega)}$, where $\varepsilon^*(\omega)$ is the complex dielectric permittivity. It consists of real (*ReM*) and imaginary (*ImM*) components, which can be derived from the dielectric permittivity:

$$ReM(\omega) = \frac{\varepsilon'(\omega)}{\varepsilon'^2(\omega) + \varepsilon''^2(\omega)} \quad (1)$$

$$ImM(\omega) = \frac{\varepsilon''(\omega)}{\varepsilon'^2(\omega) + \varepsilon''^2(\omega)} \quad (2)$$

ReM is related to stored energy, while *ImM* is linked to energy

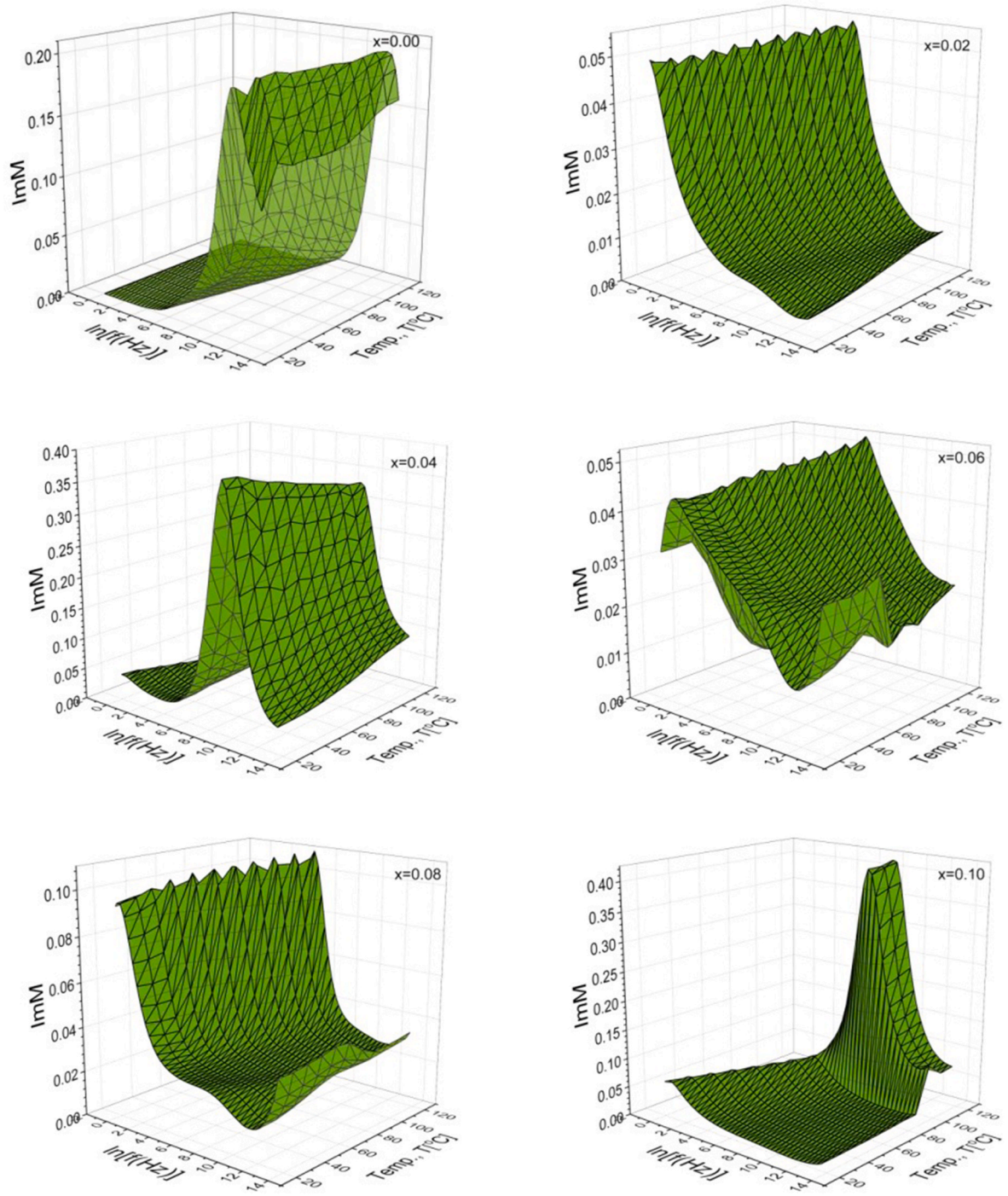

Fig. 7. 3D plot of the *f* - and T-dependent imaginary modulus (ImM) of $CoFe_{2-4x}Se_{3x}O_4$ NPs.

dissipation within the material.

Fig. 6 presents a 3D plot of the real modulus (*ReM*) of $CoFe_{2-4x}Se_{3x}O_4$ NPs, synthesized hydrothermally, with respect to *f* and T for Se^{4+} ion substitution ratios ranging from x = 0.02 to 0.10. Notably, the real modulus shows an interesting decrease along the *f* axis for x = 0.04, while other substitution ratios exhibit similar trends, except for x = 0.10. The *f* dependence of the real modulus is less pronounced compared to the high-*f* and high-T sides as shown in the plot, with peak formation clearly occurring in the x = 0.10 plot for these parameters.

Fig. 7 displays the 3D plot of the imaginary modulus (*ImM*) for the same material, with respect to *f* and T, for x = 0.02 to 0.10. The imaginary modulus shows interesting variations along the *f* axis for all Se^{4+} ion substitution ratios, with some similar trends observed in other Co-SFs, except for x = 0.04 and x = 0.10. The *f* dependence of the imaginary modulus is less pronounced compared to the high-T side, as shown in the corresponding plot. Peaks are observed in the x = 0.10 plot for these parameters, with another intriguing trend for x = 0.04. The peak value of ImM for x = 0.04 is observed at a medium *f* of around 9.8 kHz for all Ts, while a similar trend for x = 0.10 is recorded only at around 3.6 kHz at high Ts. The pronounced nature of the imaginary modulus for the substitution ratios is noteworthy.

Se^{4+} ion substitution might modify the hopping mechanism of charge carriers (e.g., between Fe^{3+} and Fe^{2+}, affecting the relaxation times and, consequently, the electric modulus. In Co-SPNPs, grain boundaries significantly impact the dielectric response. Se^{4+} ion might influence the grain size and boundary properties, altering the overall electric modulus. In the *ImM* versus *f* plot, one typically observes peaks corresponding to different relaxation processes. Se ion substitution could shift these peaks due to changes in the Ea required for dipolar relaxation.

The T dependence of complex electric modulus can reveal further details about the relaxation dynamics. An increase in T decreases relaxation time, leading to a shift in the *ImM* peak to higher frequencies. Se^{4+} ion substitution might modify this behavior, indicating changes in the Ea for dipolar relaxation. Therefore, impedance spectroscopy can provide additional insights into the relaxation mechanisms and conductivity behavior. When combined with modulus analysis, it helps in distinguishing between grain and grain boundary contributions to the overall dielectric response.

The combined analysis of the Nyquist plots (impedance) and modulus formalism can help in understanding the impact of Se^{4+} ion substitution on electrical conduction and relaxation processes in the material. Se^{4+} ion might enhance the electrical conductivity of Co-SFs due to increased polaron hopping or improved grain boundary conductivity. The presence of Se^{4+} ion could lead to a reduction or increase in the relaxation time depending on whether it enhances or hinders charge carrier mobility. Some shifts in the modulus peaks could be observed with changing *f* and T, reflecting the modified dynamics due to Se^{4+} ion substitution. Thus, Se^{4+} ion substitution in Co-SFs synthesized via hydrothermal methods is likely to significantly affect the electric modulus, reflecting changes in the dielectric and conductive properties of the ferrites. Detailed analysis of electric modulus, along with complementary techniques like impedance spectroscopy, will provide a comprehensive understanding of these effects.

3.5. Complex impedance

3.5.1. ImZ/ReZ ratio analysis

The ImZ/ReZ ratio of complex impedance in $CoFe_{2-4x}Se_{3x}O_4$ NPs reveals essential understandings into the electrical and dielectric properties of material from low Hz to kHz and Ts (20 °C–120 °C) (see Fig. 8). This ratio analysis helps identify changes in conduction mechanisms, polarization effects, and the response of the resistive and reactive components of the material.

The Se ion substitution has a pronounced effect on the ImZ/ReZ ratio, shifting the peak frequencies as a function of both substitution levels and T. For x = 0.04, the ratio exhibits a pronounced peak at 63 Hz at 20 °C, shifting to 476 Hz as the T rises to 120 °C. The peak value decreases significantly with increasing T, indicating changes in the material's conduction behavior. For x = 0.06 and x = 0.08, similar trends are observed. However, the peak frequencies differ. For x = 0.06, the peak at 104 kHz disappears above 80 °C, while for x = 0.08, the peak shifts from 94 kHz to 145 kHz as T rises, with peak broadening indicating modified dielectric behavior. For x = 0.10, peaks shift from 94 kHz at 20 °C to 203 kHz at 90 °C. Above 100 °C, no significant peaks are observed, though minor variations suggest some activity at high Ts, particularly between 100 and 120 °C.

At low Ts, resistive behavior dominates (low ImZ/ReZ ratio) due to fewer thermally activated charge carriers. As the T increases, the ratio shifts toward higher frequencies due to thermally activated conduction processes. The balance between resistive and reactive components becomes more evident at medium frequencies. Here, polarization and dielectric relaxation phenomena begin to dominate, creating a transition in the ImZ/ReZ ratio. With higher Se substitution, the *f* at which these transitions occur shifts, indicating changes in the conduction mechanism. At high frequencies (above 150 kHz), capacitive behavior becomes prominent, and the ImZ/ReZ ratio stabilizes. Se substitution can either enhance or suppress this high-*f* response, reflecting the material's intrinsic capacitive properties and its influence on the dielectric relaxation processes.

At low Ts, impedance is high, with resistive components dominating due to limited charge carrier hopping. At higher Ts, more charge carriers are thermally activated, leading to reduced resistive behavior (ReZ decreases). This results in a shift of the ImZ/ReZ ratio toward higher frequencies, with noticeable peaks indicating relaxation processes becoming more prominent.

For low substitution ratios ($x \leq 0.04$), the effect on impedance is moderate, and the ImZ/ReZ ratio follows typical trends for spinel ferrites, with relatively small shifts in peak *f*. For higher substitution ratios ($x > 0.04$), the material's structure undergoes more substantial changes, altering the dielectric relaxation times, conduction mechanism, and *f* response. Higher substitutions lead to more pronounced changes in the ratio, shifting the peak *f* and altering the resistive and reactive balance.

Consequently, the ImZ/ReZ ratio analysis of $CoFe_{2-4x}Se_{3x}O_4$ ferrites as a function of *f*, T, and Se substitution provides valuable information on the conduction and dielectric properties. The analysis highlights how Se ion substitution modifies the *f* response, dielectric relaxation, and overall impedance behavior of the material. These changes, influenced by T and substitution levels, shed light on the underlying conduction mechanisms and structural-electrical relationship of the material.

3.5.2. Cole-Cole plot analysis

This section examines the influence of Se^{4+} ion substitution on the complex impedance properties of $CoFe_2O_4$ NPs synthesized via the hydrothermal method. NPs are known for their unique electrical, magnetic, and dielectric properties, making them suitable for various applications, including sensors, catalysts, and electromagnetic devices [20,30]. In particular, the substitution of Se^{4+} ions into the spinel grain lattice of $CoFe_2O_4$ has been proposed to tailor these properties. So, the research focuses on how varying Se^{4+} ion substitution ratios ($0.02 \leq x \leq 0.10$) and different Ts (20, 70 and 120 °C) impact the impedance behavior of the materials. Nyquist plots, which are graphical representations of complex impedance data, are used to analyze this behavior. These plots, where the real part of impedance (*ReZ*) is plotted against the negative imaginary part (*-ImZ*), provide insight into the resistive and capacitive characteristics of the material.

The Nyquist plot of complex impedances (*-ImZ vs. ReZ*) for hydrothermally synthesized $CoFe_{2-4x}Se_{3x}O_4$ NPs, is shown in Fig. 9. This plot covers a T range from 20 to 120 °C, with 20 °C intervals, for frequencies up to 3.0 MHz. It is evident from the plot that both components of the complex impedance decrease as the T increases. Additionally, these impedance components are highly dependent on the Se ion substitution ratios. The diameters and shapes of the semicircular arcs in the Nyquist

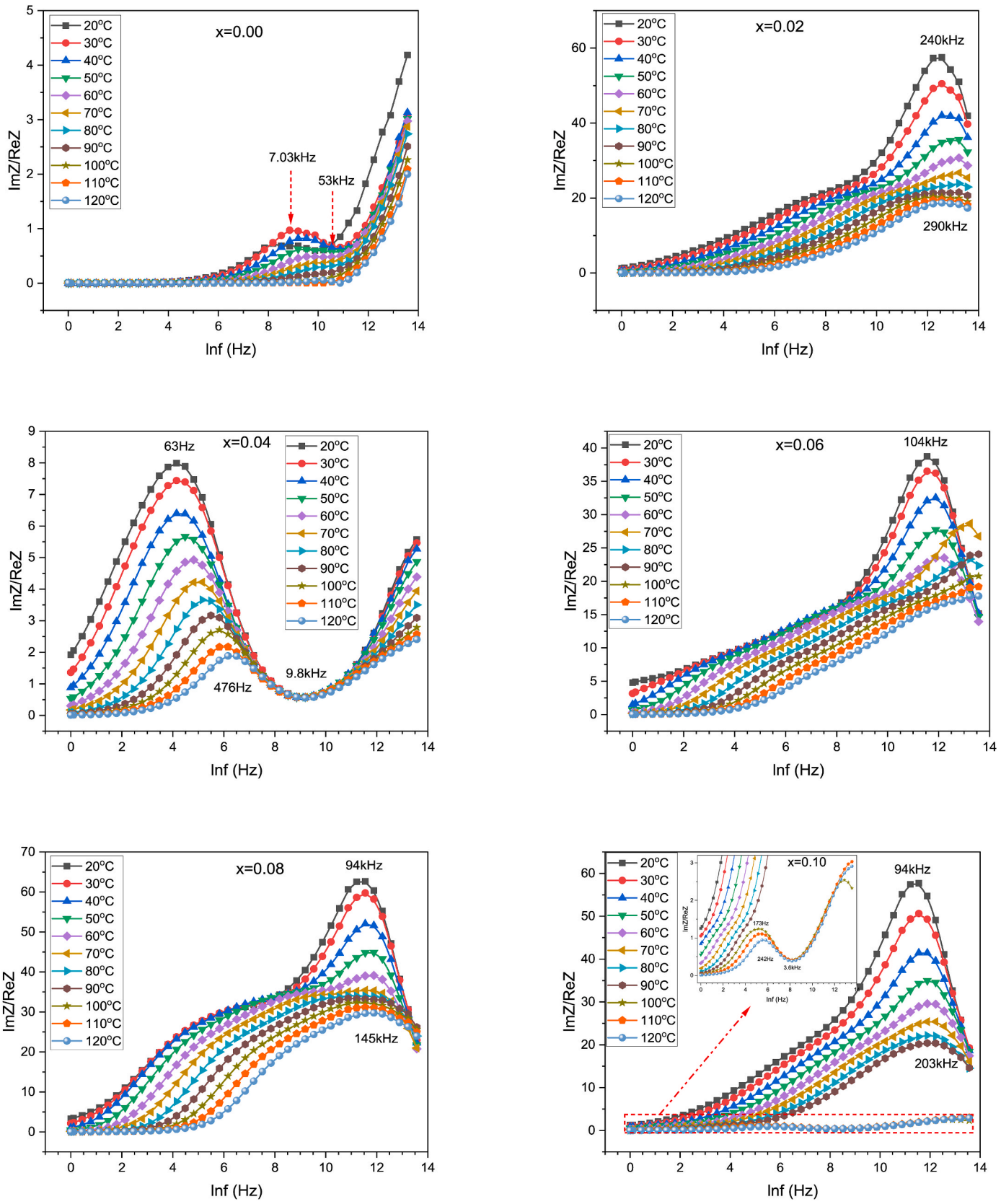

Fig. 8. The ImZ/ReZ ratio of the complex impedance for $CoFe_{2-4x}Se_{3x}O_4$ NPs across a range of frequencies up to 1 MHz between 20 and 120 °C).

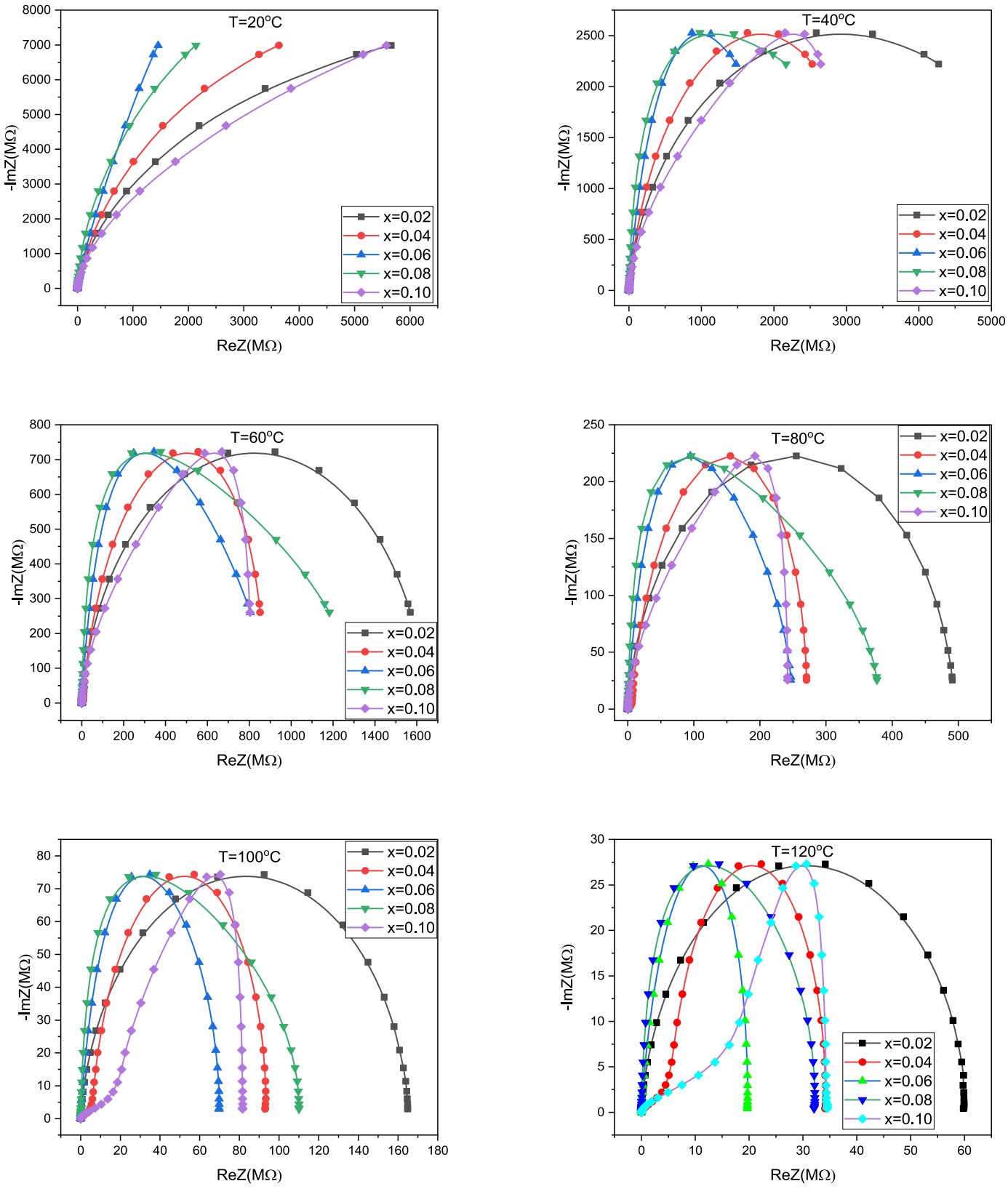

Fig. 9. Nyquist plot (-ImZ vs. ReZ) of complex impedances for hydrothermally synthesized $CoFe_{2-4x}Se_{3x}O_4$ NPs between 20 and 120 °C.

plots vary significantly with both the T and substitution ratios, indicating a strong dependence on these parameters. Notably, the diameter of the semicircular arcs reduces as the T increases.

Fig. 10 further illustrates this behavior through the Cole-Cole plot (*-ImZ vs. ReZ*), which provides a detailed view of the complex impedance characteristics of $CoFe_{2-4x}Se_{3x}O_4$ NPs at various Ts within the same range. This plot, which also accounts for frequencies up to 3.0 MHz and Se^{4+} ion substitution ratios from 0.02 to 0.10, offers a comprehensive

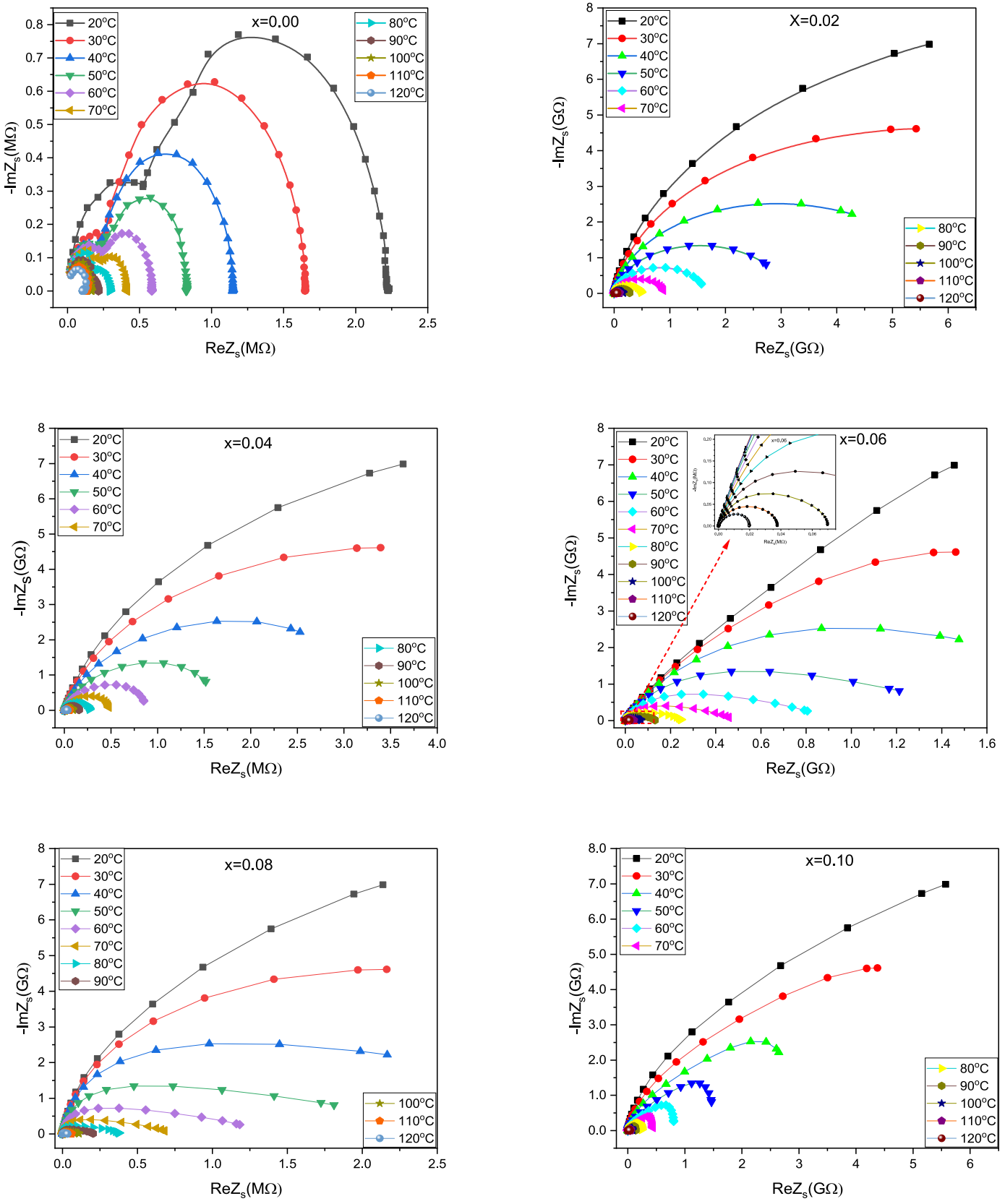

Fig. 10. Cole-Cole plot (-ImZ vs. ReZ) of complex impedances for $CoFe_{2-4x}Se_{3x}O_4$ NPs up to 3.0 MHz between 20 and 120 °C.

perspective on how substitution ratios and T influence the impedance properties of the material.

Fig. 11 in the study presents Nyquist plots and their corresponding equivalent circuit models for the $CoFe_{2-4x}Se_{3x}O_4$ NPs. Specifically, Fig. 11a shows the Nyquist plots for x between 0.02 and 0.10 at 20 and 70 °C. As the Se^{4+} ion substitution ratio increases, the size of the semicircles in the Nyquist plots generally changes, indicating modifications in charge traNPer resistance and overall conductivity. Additionally, a T-dependent decrease in resistance is observed, suggesting thermally activated conduction, a characteristic consistent with semiconductor materials.

Fig. 11b depicts Nyquist plots for the sample with a fixed substitution ratio of x = 0.02, measured at three different Ts: 20, 70 and 120 °C. The plots show that the semicircle diameter decreases as the T increases, further supporting the notion of thermally activated conduction mechanisms within the material. At higher Ts, the material exhibits lower resistance, facilitating easier charge carrier movement.

Fig. 11c illustrates the equivalent circuit model used to fit the complex impedance data, which includes *resistors, capacitors*, and possibly *constant phase elements* (*CPEs*). This model accurately represents the impedance behavior of the ferrite, with the variation in circuit component values providing insight into the underlying physical processes, such as charge traNPer dynamics and polarization effects.

The study identifies the best-fit circuit model for the sample with x = 0.02 as *R(RC)(QR)(RC)* across all Ts within the *f* range of 1.0 Hz–3.0 MHz. However, for higher substitution ratios (x > 0.04), the data could not be fitted to any known model in the *ZSim software*, indicating complex impedance behavior that requires further investigation.

Tables 1 and 2 in the study provide detailed fitting parameters. Table 1 lists the parameters for the sample with x = 0.02, showing how

Table 1
Fitting parameters for $CoFe_{2-4x}Se_{3x}O_4$ (x = 0.02) NPs at various Ts.

T (°C) →	20	70	120
$R_0(\Omega)$	4.3 M	0.128	58.5
C_1(F)	3.5n	122n	1.23μ
$R_1(\Omega)$	0.23	31	1.1 M
CPE,Yo [S-sec^n]	7.8p	1.1n	3.7μ
***f* power, n (0<n<1)**	Too small	~0.0	0.344
$R_2(\Omega)$	2.7T	17G	2.8 M
C_3(F)	46n	481 μ	544n
$R_3(\Omega)$	9.0G	165 M	9.52 M

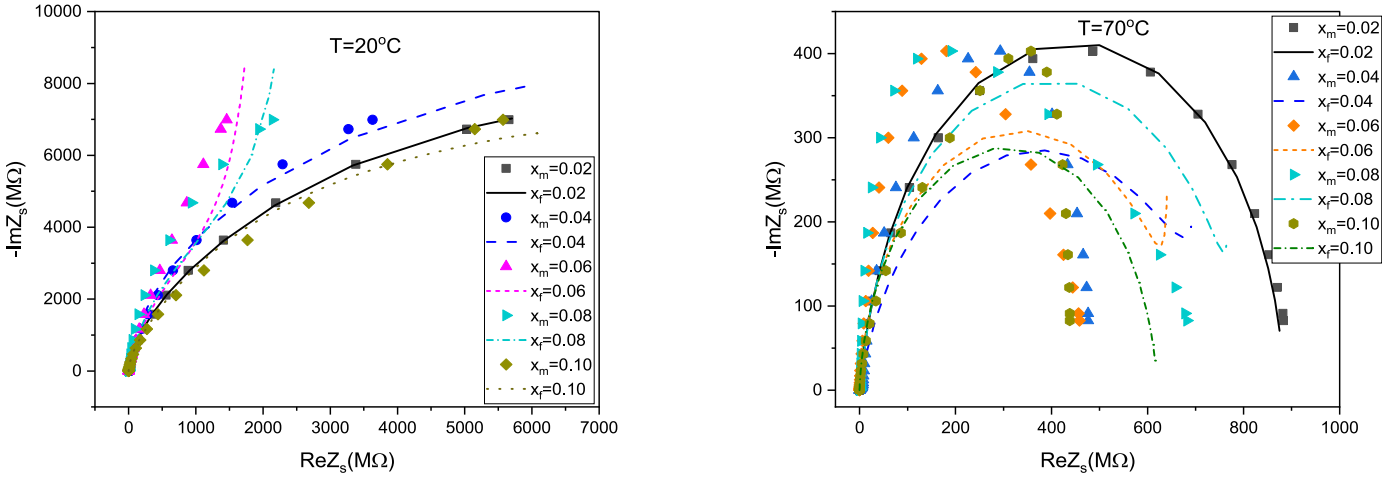

(a)

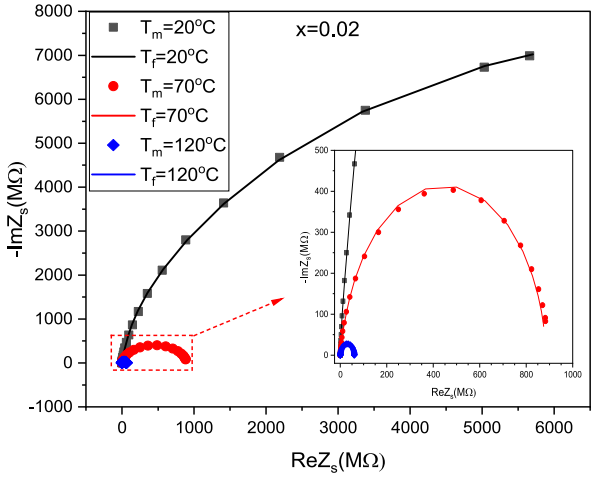

(b)

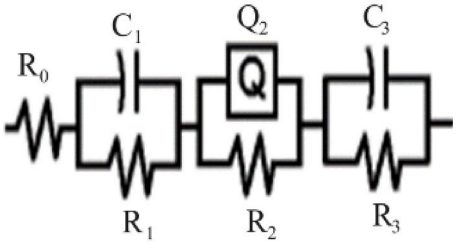

(c)

Fig. 11. Nyquist plots and equivalent circuit models for $CoFe_{2-4x}Se_{3x}O_4$ NPs.

Table 2
Fitting parameters for various substitution ratios at 20 °C.

x →	0.02	0.04	0.06	0.08	0.10
R_0(Ω)	4.3 M	97	382	6.6 M	4.3 M
C_1(F)	3.5n	338μ	~0	1.95n	4.1n
R_1(Ω)	0.23	29k	0.02	0.1	0.25
CPE,Yo [pS-sec^n]	78	230	31	42	83
***f* power, n (0<n<1)**	~0.0	0.69	0.94	~0.0	~0.0
R_2(Ω)	2.7T	16.6G	1.8G	3.8T	2.7T
C_3(F)	46n	15p	20p	47.4n	43.5n
R_3(Ω)	9.0G	9.5G	7.4T	8.7G	8.6G

components like resistor R_1 and capacitor C_1 increase with T, while others, like ***CPE*** and resistor R_2, exhibit more complex dependencies. Table 2 provides fitting parameters at 20 °C for all Se^{4+} substitution ratios, highlighting fluctuations in resistor and capacitor values depending on the substitution ratio.

Accordingly, the study demonstrates that Se^{4+} ion substitution in $CoFe_2O_4$ NPs significantly affects the electrical and dielectric properties of the material. The impedance behavior, as revealed by the Nyquist plots and equivalent circuit modeling, is highly dependent on both the substitution ratio and T [31]. These findings offer valuable insights into optimizing spinel ferrite nanoparticles for technological applications, though further research is needed to explore the impedance behavior of samples with higher substitution ratios and refine the equivalent circuit models for these complex systems.

In the literature, $CoFe_{2-4x}Se_{3x}O_4$ NPs are noted for their enhanced electrical and magnetic properties due to the unique role of Se^{4+} ion in modifying the electronic structure. Se^{4+} ion substitution tends to decrease resistivity and increase the dielectric constant, making these materials promising for applications in sensors, magnetic devices, and catalysis [30,31]. The observed trends in the Nyquist plots align with reports that Se^{4+} ion substitution improves charge transport properties, likely due to the introduction of additional charge carriers and a reduction in grain boundary resistance.

The selection of three specific temperatures—low, medium, and high—in the Cole-Cole analysis (Table 1) was made to comprehensively evaluate the relaxation dynamics and dielectric behavior of $CoFe_{2-4x}Se_{3x}O_4$ (x = 0.02) NPs. These temperatures were chosen to capture the full spectrum of thermal effects on relaxation times and polarization mechanisms, providing insights into how Se^{4+} substitution influences the material's response under varying thermal conditions. The inclusion of all substitution ratios at a standard temperature of 20 °C (Table 2) ensures a baseline comparison, while the analysis at distinct temperature regimes highlights transitions in conduction and relaxation processes critical for understanding the material's potential applications in electronic and energy storage devices.

To critically evaluate why temperature and Se ion-substitution ratios influence the electrochemical, electrical, and dielectric properties of hydrothermally synthesized Se-substituted Co-SFs, several key points must be addressed with concise justifications:

Se substitution in Co-SFs alters the crystal structure by replacing oxygen or iron sites, thereby modifying the charge distribution and interactions between Co and Fe ions. This structural modification directly impacts charge carrier mobility, which, in turn, affects both electrical conductivity and dielectric properties. Furthermore, Se substitution introduces changes to the electronic structure of Co-SFs by creating new defect states or influencing the valence states of Co and Fe ions. These changes modify the material's electrochemical behavior and its ability to conduct electricity.

Temperature also plays a critical role in influencing these properties. As temperature increases, the thermal energy available to charge carriers rises, enhancing their mobility and conductivity. For Se-substituted Co-SFs, the presence of Se can modulate this temperature effect by altering the activation energy required for conduction. At elevated temperatures, variations in defect states or potential phase transitions within the material can further affect its electrochemical performance.

In addition, selenium substitution significantly impacts the redox properties of Co-SFs, potentially enhancing their electrochemical performance for energy storage applications such as batteries and supercapacitors. A higher Se substitution ratio may introduce new redox-active sites or improve charge transfer processes, which directly influence electrical conductivity and dielectric behavior. Moreover, Se incorporation can modify the surface chemistry, promoting improved ion diffusion and enhancing the reversibility of electrochemical reactions.

The dielectric response of Co-SFs is also influenced by Se substitution, particularly in terms of polarization behavior and dielectric loss. Changes in polarization mechanisms, including ionic and electronic polarization, lead to variations in the dielectric constant and loss factor, both of which are highly temperature-dependent. The Se ratio allows for fine-tuning of these properties, either enhancing or suppressing dielectric performance based on its effect on polarization dynamics.

In conclusion, the combined influence of temperature and Se substitution on the electrochemical, electrical, and dielectric properties of Co-SFs is primarily due to their effects on charge carrier dynamics, structural modifications, and phase transitions. Se substitution improves electrical conductivity and dielectric response by altering the electronic structure, while temperature affects these properties by modulating charge carrier mobility and material behavior. Understanding the interplay between Se content and temperature is crucial for optimizing the material's performance in diverse applications, particularly in the field of energy storage and electronic devices.

4. Conclusion

The study concludes that Se^{4+} ion substitution in $CoFe_2O_4$ NPs significantly affects the electrical and dielectric properties of SF material. Nyquist plots and equivalent circuit modeling indicate that the substitution ratio and T critically influence the impedance characteristics, with higher substitution and T enhancing conductivity. The research demonstrates that Se^{4+} ions improved DC and AC conductivity, enhance Ea, and modify dielectric properties such as the dielectric constant, loss tangent, and dissipation factor. These changes are linked to alterations in charge carrier mobility, polarization mechanisms, and defect structures. The ImZ/ReZ ratio analysis highlights how Se ion substitution modifies the *f* response, dielectric relaxation, and overall impedance behavior of the ferrite material. These changes, influenced by T and substitution levels, shed light on the underlying conduction mechanisms and structural-electrical relationship of the material. The findings suggest that Se^{4+}-substituted $CoFe_2O_4$ ferrites hold potential for high-T applications, sensors, electromagnetic devices, and high-*f* circuits, with the ability to fine-tune these properties for specific technological uses.

CRediT authorship contribution statement

B. Ünal: Project administration, Formal analysis, Conceptualization. **A. Baykal:** Writing – review & editing, Writing – original draft, Visualization, Validation, Supervision, Project administration, Methodology, Investigation, Formal analysis, Conceptualization. **M.A. Almessiere:** Writing – review & editing, Writing – original draft, Validation, Resources, Methodology, Formal analysis, Data curation, Conceptualization. **A. Mihmanlı:** Software, Resources, Methodology, Investigation.

Declaration of competing interest

The authors declare that they have no known competing financial interests or personal relationships that could have appeared to influence the work reported in this paper.

References

[1] O.D. Dastjerdi, H. Shokrollahi, S. Mirshekari, A review of synthesis, characterization, and magnetic properties of soft spinel ferrites, Inorg. Chem. Commun. 153 (2023) 110797.

[2] M. Kamran, M. Anis-ur-Rehman, Influence of La^{3+} substitutions on structural, dielectric and electrical properties of spinel cobalt ferrite, Ceram Int 49 (2023) 7017.

[3] S.B. Narang, K. Pubby, Nickel spinel ferrites: a review, J. Magn. Magn Mater. 519 (2021) 167163.

[4] I. Ahmad, S.M. Shah, M.N. Zafar, M.N. Ashiq, W. Tang, U. Jabeen, Synthesis, characterization and charge transport properties of Pr–Ni Co-doped $SrFe_2O_4$ spinel for high frequency devices applications, Ceram. Int. 47 (2021) 3760.

[5] I. Ahmad, S.M. Shah, M.N. Zafar, S. Ullah, A. Ul-Hamid, M.N. Ashiq, U. Jabeen, M. Shafa, A. Rahdar, Fabrication of highly resistive La–Zn co-substituted spinel strontium nanoferrites for high frequency devices applications, Mater. Chem. Phys. 259 (2021) 124031.

[6] M. Houshair, F. Zebhi, Z.J. Razi, A. Alidoust, Z. Askari, Synthesis of cobalt ferrite ($CoFe_2O_4$) nanoparticles using combustion, co-precipitation, and precipitation methods: a comparison study of size, structural and magnetic properties, J. Magn. Magn Mater. 371 (2014) 43.

[7] S. Ouaissa, A. Benyoussef, G.S. Abo, M. Ouaissa, M. Hafid, Magnetization study of cobalt ferrite by mean field approximation, Phys. Procedia 75 (2015) 792.

[8] N.A. Sdran, M. Shkir, H.E. Ali, K.V. Chandekar, Enhanced structural, optical, dielectric, and electrical properties of $CoFe_2O_4$ nanostructures: effect of variation of citric acid concentration, Ceram. Int. 50 (2024) 4673.

[9] S. Rashid, S. Perveen, S. Hafeez, S. Asad, M.Z. Khan, F. Azad, Graphene quantum dots (GQDs) decorated Co-Zn ferrite: structural, morphological, dielectric, and magnetic properties, J. Magn. Magn Mater. 570 (2023) 170548.

[10] R. Biswal, P. Yadav, P. Mishra, P. Kumar, M.K. Singh, Synthesis, structural, optical, dielectric, magnetic and magneto-dielectric properties of $CoFe_2O_4$ and Graphene Quantum Dots (GQDs) decorated $CoFe_2O_4$ hybrid nanocomposite, Mater. Chem. Phys. 318 (2024) 129271.

[11] F. Sharifianjazi, M. Moradi, N. Parvin, A. Nemati, A.J. Rad, N. Sheysi, A. Abouchenari, A. Mohammadi, S. Karbasi, Z. Ahmadi, A. Esmaeilkhanian, M. Irani, A. Pakseresht, S. Sahmani, M.S. Asl, Magnetic $CoFe_2O_4$ nanoparticles doped with metal ions: a review, Ceram. Int. 46 (2020) 18391.

[12] M.K. Surendra, S. Annapoorani, E.B. Ansar, P.H. Varma, M.R. Rao, Magnetic hyperthermia studies on water-soluble polyacrylic acid-coated cobalt ferrite nanoparticles, J. Nanoparticle Res. 16 (12) (2014) 2773.

[13] F. Ameen, N. Majrashi, Recent trends in the use of cobalt ferrite nanoparticles as an antimicrobial agent for disability infections: a review, Inorg. Chem. Commun. 156 (2023) 111187.

[14] V. Balasubramani, V. Mowlika, A. Sivakumar, N. Al Sdran, F. Maiz, M. Shkir, Design and investigation of Sono-chemical synthesis of pure and Sn doped $CoFe_2O_4$ nanoparticles and their structural and magnetic properties, Inorg. Chem. Commun. 155 (2023) 111015.

[15] M. Hashim, M. Raghasudha, S.S. Meena, J. Shah, S.E. Shirsath, S. Kumar, D. Ravinder, P. Bhatt, R. Kumar, R. Kotnala, Influence of rare earth ion doping (Ce and Dy) on electrical and magnetic properties of cobalt ferrites, J. Magn. Magn Mater. 449 (2018) 319.

[16] S. Ravi Kumar, G. Vishnu Priya, B. Aruna, M.K. Raju, D. Parajuli, N. Murali, R. Verma, K.M. Batoo, P.V. Rajesh Kumar, L. Narayana, Influence of Nd^{3+} substituted $Co_{0.5}Ni_{0.5}Fe_2O_4$ ferrite on structural, morphological, dc electrical resistivity and magnetic properties, Inorg. Chem. Commun. 136 (2022) 109132.

[17] G. Xi, T. Zhao, L. Wang, C. Dun, Y. Zhang, Effect of doping rare earths on magnetostriction characteristics of $CoFe_2O_4$ prepared from spent Li-ion batteries, Phys. B Condens. Matter 534 (2018) 76.

[18] A. Baykal, Y. Slimani, M.A. Almessiere, A.D. Korkmaz, H. Güngünes, S. Caliskan, E. Arslan, S.E. Shirsath, Exploring the structural and magnetic properties of Se-substituted NiCuZn nanospinel ferrites, J. Mol. Struct. 1319 (2) (2025) 139487.

[19] M.A. Almessiere, A. Baykal, S. Caliskan, Y. Slimani, A. Ul-Hamid, Comparing Magnetic Characteristics of $CoSe_{3x}Fe_{2-4x}O_4$ ($x \leq 0.10$) spinel ferrite nanoparticles synthesized via Sol-Gel and Hydrothermal approaches, Nano-Structures & Nano-Objects 38 (2024) 101196.

[20] Y. Bide, M.R. Nabid, B. Etemadi, Facile synthesis and catalytic application of selenium doped graphene/$CoFe_2O_4$ for highly efficient and noble metal free dehydrogenation of formic acid, Int. J. Hydrogen Energy 41 (2016) 20147.

[21] R.N. Chikhale, V.S. Shinde, P.G. Bhatia, Investigate structural, morphological, electrical, dielectric and magnetic properties of dysprosium doped Cobalt-Nickel ferrites and their response to gamma irradiation,Nucl. Instrum, Methods Phys. Res. 550 (2024) 165320.

[22] Y.Q. Chu, B. Zhang, J. Xiang, Synthesis of nickel-based ferrite nanofibers and their static magnetic and microwave absorption properties, Adv. Mater. Res. Trans. Tech. Publ. (2013).

[23] K. Vani, N. Hari kumar, D. Ravinder, Rare earth Gd^{3+} substituted on cobalt ferrites: Structural and dielectric studies by citrate gel autocombustion method, Inorg. Chem. Commun. 160 (2024) 111920.

[24] C.Y. Mang, Z.J. Ma, J. Luo, M.J. Rao, X. Zhang, Z.W. Peng, Electromagnetic wave absorption properties of cobalt-zinc ferrite nanoparticles doped with rare earth elements, J. Rare Earths 39 (2021) 1415.

[25] M. Rashid, M.A. Khan, R.T. Rasool, H. Alhummiany, M. Arshad, G.A. Ashraf, I. Boukhris, M. Irfan, M.M. Al-Anazy, M.N. Akhtar, Influence of Ni^{2+} ions on structural, spectral and dielectric properties of Sr–Co spinel ferrites synthesized by sol-gel auto-combustion route, Ceram. Int. 50 (2024) 24679.

[26] B. Ünal, M. Almessiere, A. Demir-Korkmaz, Y. Slimani, A. Baykal, Effect of thulium substitution on conductivity and dielectric belongings of nanospinel cobalt ferrite, J. Rare Earths 38 (10) (2020) 1103.

[27] M.A. Almessiere, Y. Slimani, B. Ünal, T.I. Zubar, A. Sadaqate, A.V. Trukhanov, A. Baykal Microstructure, Dielectric and microwave features of $[Ni_{0.4}Cu_{0.2}Zn_{0.4}](Fe_{2-x}Tb_x)O_4$ ($x \leq 0.1$) nanospinel ferrites, J. Mater. Res. Technol. 9 (5) (2020) 10608.

[28] A. Baykal, Y. Slimani, M.A. Almessiere, A.D. Korkmaz, H. Güngünes, S. Caliskan, E. Arslan, S.E. Shirsath, Exploring the structural and magnetic properties of Se-substituted NiCuZn nanospinel ferrites, Ceram. Int. 49 (2023) 7017.

[29] S. Caliskan, M.A. Almessiere, A. Baykal, Y. Slimani, A first principles study on electronic structure, magnetic and optical characteristics of Se doped $CoNiFe_2O_4$ spinel ferrites, Comput. Mater. Sci. 226 (2023) 112243.

[30] S. Holm, Time domain characterization of the Cole-Cole dielectric model, J. Electr. Bioimp. 11 (1) (2020) 101.

[31] M. Šiljegović, Ž. Cvejić, S. Jankov, E. Toth, D. Herceg, P. Odry, V. Tadic, Impedance and dielectric analysis of nickel ferrites: revealing the role of the constant phase element and yttrium doping, Electronics 13 (8) (2024) 1496.